Synthesis, biological activity, and in silico studies of thieno[2,3-d]pyrimidine and thieno[2,3-d]triazine derivatives

Fatma A.A. El-Hag[a], Ahmed A. Elrashedy[a], Ayman M.K. Sweed[a], Ewies F. Ewies[b], Mansoura A. Abd-El-Maksoud[b], Magdy S. Aly[c], Sanaa M.Sh. Atta[a]

Departments of [a]Chemistry of Natural and Microbial Products, [b]Organometallic and Organometalloid Chemistry, National Research Centre, Giza, [c]Genetics Division, Department of Zoology, Faculty of Science, Beni-Suef University, Beni-Suef, Egypt

Correspondence to Fatma A.A. El-Hag (PhD), Department of Chemistry of Natural and Microbial Products, Pharmaceutical and Drug Industries Research Institute, National Research Centre, 33 El- Bohouth St. (former El Tahrir St.), Dokki, P.O. 12622, Giza, Egypt.
Tel: +20 122 357 1676/+20 115 793 8447;
fax: + 20 233 370 931;
e-mail: fatmaabdaleem@yahoo.com

Received: 14 June 2022
Revised: 2 July 2022
Accepted: 4 July 2022
Published: 21 September 2022

Egyptian Pharmaceutical Journal 2022, 21:360–375

Background
The chemistry of condensed heterocyclic compounds has emerged in numerous reports for their diverse biological properties and drug discovery. Pyrimidine and triazine scaffolds have been utilized as therapeutic agents in many medicinal applications. Many research groups have designed and synthesized pyrimidine moieties as they are incorporated in nucleic acid bases.

Objective
In this report, we have designed and synthesized a variety of 2-mercaptothieno pyrimidine and thienotriazine derivatives and 2-mercaptothienopyrimidines conjugated with sugar moiety. The newly synthesized compounds were tested for their biological activity against breast (MCF-7), liver (HepG-2), and prostate (PC-3) cancer cell lines as well as a normal cell line (human normal melanocyte, HFB4) and were also analyzed for in silico studies to determine their potential.

Materials and methods
A variety of 2-mercaptothienopyrimidine and thienotriazine derivatives were prepared via cyclization of ethyl 2-amino-4,5,6,7-tetrahydrobenzo[b]thiophene-3-carboxylate **(1)** and 2-amino-*N*-phenyl-4,5,6,7-tetrahydrobenzo[*b*]thiophene-3-carboxamide **(9)**. Two derivatives of 2-mercaptothienopyrimidines conjugated with sugar moiety were also prepared. The products were screened for their biological activity against breast (MCF-7), liver (HepG-2), and prostate (PC-3) cancer cell lines as well as the normal cell line (human normal melanocyte, HFB4) in comparison with the known anticancer drug 5-fluorouracil using the MTT assay.

Results and conclusion
The results indicated that most of the tested compounds exhibited no activity against the growth of HFB4. Compounds **5, 8, 10, 12,** and **14** revealed effective antiproliferative activity against MCF-7 cell lines with IC_{50} of 4.6, 6.2, 5.4, 7, and 3.25 μg/ml, respectively, compared with 5-fluorouracil (IC_{50} of 3.97 μg/ml). In the same sense, the evaluation of cytotoxic effect of the tested compounds against human liver HepG-2 cancer cell lines revealed that compounds **5, 8, 10, 12,** and **14** showed cytotoxic activity close to that of the standard drug (IC_{50} values of 5.77 ±0.99, 7.23±0.98, 4.42±1.32, 7.9±0.90, and 5.1±11.28 μg/ml, respectively, vs. 4.27 ±0.58 μg/ml for 5-fluorouracil). Free binding energy was estimated by docking and MM-GBSA calculation. Molecular dynamics simulation followed by MM-GBSA calculation was correlated to the cytotoxic effect. Compound 14 illustrated the highest MM-GBSA value (–20.38) and the best cytotoxic effect.

Keywords:
cytotoxic agents, heterocycles, molecular dynamics, pyrimidine, triazine

Egypt Pharmaceut J 21:360–375

1687-4315

Introduction

The chemistry of condensed heterocyclic compounds has emerged in numerous reports for their diverse biological properties and drug discovery. Pyrimidine and triazine scaffolds have been used as therapeutic agents in many medicinal applications [1–3]. Many research groups have designed and synthesized pyrimidine moieties [2,4,5], as they are incorporated in nucleic acid bases. It has also been reported that pyrimidine bases are biologically active by themselves. Among the condensed pyrimidines and triazines, cyclo-thieno[2,3-d]pyrimidine [6–8], and cyclo-thieno[2,3-d] [1,2,3] triazine [9] have significant and versatile biological properties, which include anticancer [10,11], anti-inflammatory [12], anti-oxidant [13], kinase inhibition, antimicrobial [14], and antiviral. Herein, in our study, a general

approach has been followed for the synthesis of thieno [2,3-d] pyrimidine and thieno[2,3-d] [1,2,3] triazine derivatives, which involves the condensation of an O-amino carbonyl thiophene with different reagents in different conditions. In our study, 2-mercaptothieno [2,3-d] pyrimidine [15] was successfully conjugated with different reagents to get novel derivatives. These compounds were tested for biological activity against three different human cancer cell lines: MCF-7, HepG-2, and PC-3, as well as a normal cell line (human normal melanocyte, HFB4), in contrast to the well-known anticancer drug:

MTT test for 5-fluorouracil.

Materials and methods

Chemistry

Melting points were determined in open glass capillaries using an Electrothermal IA 9000 series digital melting point apparatus (Electrothermal, Essex, UK) and are uncorrected. The infrared (IR) spectra were measured in KBr pellets with a Perkin–Elmer Infracord Spectrophotometer model 157 (Grating). The 1H and 13C NMR spectra were recorded in CDCl3 on a JEOL-500 MHz spectrometer, and the chemical shifts were recorded in δ values relative to TMS. The mass spectra were performed at 70 eV on a Shimada GCS-OP 1000 Ex Spectrometer provided with a data system. Elemental analyses were performed using ElmenterVaru EL Germany Instrument. The reported yields are based upon pure materials isolated. Solvents were dried/purified according to conventional procedures.

Ethyl 2-amino-4,5,6,7-tetrahydrobenzo[b]thiophene-3-carboxylate (1)

Compound **1** was synthesized by the method reported in the literature [16]. It had M.P. of 115–117°C (Lit. 115°C); MS (*m/z*): M+ 226 (15%); and analysis for $C_{11}H_{15}NO_2S$ (225.08) revealed the following: Calcd.: %C, 58.64; H, 6.71; N, 6.22; S, 14.23, and found: %C, 58.82; H, 6.55; N, 6.30; S, 14.12.

Ethyl 2-(3-benzoylthioureido)-4,5,6,7-tetrahydrobenzo[b] thiophene-3-carboxylate (2)

A mixture of compound **1** (100 mmol, 3.9 g) and (100 mmol, 12 g) benzoyl isothiocyanate was stirred at r.t. for 20 h to afford a solid product, which was poured onto crushed ice and collected by filtration.

N.B. *Benzoyl isothiocyanate prepared by adding ammonium isothiocyanate (0.01 mol) to a solution of benzoyl chloride (0.01 mol) in 1,4-dioxane (100 ml) was refluxed for 1 h followed by isolation of ammonium chloride as a byproduct.*

Product **2** was separated as yellow crystals, with yield of 75% (EtOH); M.P. of 162–164°C (lit. 160°C [17]); IR (KBr, cm^{-1}): 3283, 3171 (NH), 1690, 1665 (C=O), 1250 (C=S), 1610 (C=C); ^{1}H NMR (500 MHz, DMSO-D6) δ8.37, 8.30 (2 s, 2H, 2 NH), 7.45–7.35 (m, 5H, CHarom.), 4.29 (q, 2H, CH_2), 2.80, 2.60 (m, 4H, 2 CH_2), 1.78 (m, 4H, 2 CH_2), 1.38 (t, J=7.0 Hz, 3H, CH_3); ^{13}C NMR (125 MHz, DMSO-D6) δ171.6 (S=O), 165.8 (C=O), 161.2 (cyclic=C-S), 155.9 (C=O), 140.2, 134.2, 131.1, 130.3, 128.0, 127.5, 117.2, 112.6 (aromatic, C-H), 62.7 (CH_2), 25.0, 24.1, 23.1, 21.0 (CH_2), 15.5 (CH_3); and MS (*m/z*): M^+ 388 (20%). Analysis for $C_{19}H_{20}N_2O_3S_2$ (388.09) revealed the following: Calcd.: % C, 58.74; H, 5.19; N, 7.21; S, 16.50, and found: % C, 58.82; H, 5.26; N, 7.33; S, 16.35.

2-Mercapto-5,6,7,8-tetrahydrobenzo [4,5]thieno[2,3-d] pyrimidin-4(3H)-one (3)

Product 3 was separated as brown crystals, with yield of 79% (EtOH); M.P. of 238–240°C [Lit. 231–233°C [18]; IR (KBr, cm^{-1}): 3293, 3131 (NH), 1690, 1665 (C=O), 1650 (C=S), 1610 (C=C); ^{1}H NMR (500 MHz, DMSO-D6) δ5.96 (s, 1H, NH), 3.13 (s, 1H, SH), 2.89–2.75 (m, 2H, CH_2), 2.65–2.57 (m, 2H, CH_2), 1.75–1.60 (m, 4H, 2 CH_2). ^{13}C NMR (125 MHz, DMSO-D6) δ179.8 (C-SH), 158.4 (C=O), 153.7 (cyclic=C-S), 134.1, 129.9, 119.2 (quaternary C), 25.5–23.6 (2 CH_2); and MS (*m/z*): M-2 236 (5%). Analysis for $C_{10}H_{10}N_2OS_2$ (238.02) revealed the following: Calcd.: % C, 50.40; H, 4.23; N, 11.75; S, 26.90, and found: % C, 50.55; H, 4.33; N, 11.61; S, 26.72.

(2R,3R, 5R,6S)-2-(acetoxymethyl)-6-((4-oxo-3,4,5,6,7,8-hexahydrobenzo[4,5]thieno[2,3-d]pyrimidin-2-yl)thio) tetrahydro-2H-pyran-3,4,5-triyl triacetate (5)

Overall, 15 mmol of NaH was added slowly to a solution of compound **3** (10 mmol) in DMF (20 ml), and the reaction mixture was stirred for 30 min at r.t. Then, 10 mmol of (2R, 3R, 5R, 6R)-2-(acetoxymethyl)-6-bromotetrahydro-2*H*-pyran-3,4,5-triyl triacetate (**4**) in DMF was added drop-wise to the reaction mixture for 30 min, with continuous stirring at r.t. until completion (TLC). Then, the reaction mixture was poured into ice water to afford a product, which was collected by filtration, dried, and crystallized from an appropriate solvent to give compound **5**.

Product **5** was separated as brown crystals, with yield 80% (EtOH); M.P. of 227–229°C; IR (KBr, cm^{-1}):

3224 (NH), 1762, 1682 (C=O), 1610 (C=C), and 1599 (C=N); ^{1}H NMR (500 MHz, DMSO-D6) δ6.01 (s, 1H, NH), 5.79 (dd, *J*=9.5, 2.7 Hz, 1H, cyclic CH), 5.44 (*d*, *J*=0.9 Hz, 1H, cyclic CH-S), 5.24 (dd, *J*=2.6, 1.1 Hz, 1H, cyclic CH), 4.89 (dd, *J*=9.6, 6.1 Hz, 1H, cyclic CH), 4.48–4.42 (m, 1H, Ha, CH_2), 4.32 (*d*, *J*=6.1 Hz, 1H, cyclic CH), 4.11–4.04 (m, 1H, Hb, CH_2). 2.87–2.77 (m, 2H, CH_2), 2.64–2.56 (m, 2H, CH_2), 2.01, 1.98, 1.96, 1.91 (4s, 12H, 4 OAc), 1.73–1.61 (m, 4H, 2 CH_2); ^{13}C NMR (125 MHz, DMSO-D6) δ171.8 (3 C=O), 169.4 (C=O), 156.4 (C=O), 152.7 (cyclic =C-S-), 134.1, 119.9, 112.2 (3 quaternary C), 74.3, 73.8, 70.2, 70.1, 69.9 (5 pyran C), 60.2 (CH_2), 25.5–23.6 (2 CH_2), 21.3–20.5 (CH_3); and MS (*m/z*): M^{+1} 567 (5%). Analysis for $C_{24}H_{28}N_2O_{10}S_2$ (568.12) revealed calcd.: % C, 50.70; H, 4.96; N, 4.93; S, 11.28, and found: % C, 50.95; H, 4.72; N, 4.62; S, 11.45.

2-(((2S,3R,5S,6R)-3,4,5-trihydroxy-6-(hydroxymethyl) tetrahydro-2H-pyran-2-yl)thio)-5,6,7,8-tetrahydrobenzo [4,5]thieno[2,3-d]pyrimidin-4(3H)-one (6)

A mixture of compound **5** (0.5 mmol) in 30 ml of MeOH, triethylamine (TEA, 1 ml), and a few drops of water was stirred overnight at room temperature. The solvent was then removed under vacuum, and the residue was washed with chloroform. The remaining residue was crystallized from ethanol to yield yellow crystals of product **6**.

Product **6** was separated as yellow crystals, with yield 90% (EtOH); M.P. of 188–200°C; IR (KBr, cm^{-1}): 3400–3330 (very broad OH), 3220 (NH), 1685 (C=O), 1612 (C=C), 1598 (C=N); ^{1}H NMR (500 MHz, DMSO-D6) δ6.05 (s, 1H, NH), 5.41 (d, *J*=5.5 Hz, 1H, OH), 5.32 (d, *J*=5.6 Hz, 1H, OH), 5.12 (d, *J*=5.1 Hz, 1H, OH), 4.56 (d, *J*=6.1 Hz, 1H, OH), 4.47–4.40 (m, 1H, Ha, CH_2), 4.11–4.04 (m, 1H, Hb CH_2), 3.67–3.88 (m, 5H, CH pyran), 2.85–2.76 (m, 2H, CH_2), 2.60–2.56 (m, 2H, CH_2),1.73–1.61 (m, 4H, 2 CH_2); ^{13}C NMR (125 MHz, DMSO-D6) δ171.8 (3 C=O), 169.4 (C=O), 156.4 (C=O), 152.7 (cyclic =C-S-), 134.1, 119.9, 112.2 (3 quaternary C), 74.3, 73.8, 70.2, 70.1, 69.9 (5 pyran C), 60.2 (CH_2), 25.5–23.6 (2 CH_2), 21.3–20.5 (CH_3); and MS (*m/z*): M^{+1} 400 (5%), 199 (100%).

Analysis for $C_{16}H_{20}N_2O_6S_2$ (400.08) revealed calcd.: % C, 47.99; H, 5.03; N, 7.00; S, 16.01, and found: % C, 47.82; H, 5.10; N, 7.05; S, 16.12.

5,6,7,8-Tetrahydrobenzo[4,5]thieno[2,3-d]pyrimidine-2,4-diol (7)

Overall, 1 mmol of compound **1** was fused with 1 mmol urea at 200°C. The mixture became a clear yellow color. The reaction mixture was dissolved in 1 N sodium hydroxide and acidified with 1 N HCl. The product **7** was crystallized from water.

Product **7** was separated as colorless crystals, with yield 63 (EtOH) %; M.P. of 221–223°C; IR (KBr, cm^{-1}): 3400–3330 (very broad OH), 1619 (C=C), 1599 (C=N); ^{1}H NMR (500 MHz, DMSO-D6) δ9.01 (s, 2H, 2 OH), 2.83–2.67 (m, 4H, 2 CH_2), 1.73–1.61 (m, 4H, 2 CH_2); ^{13}C NMR (125 MHz, DMSO-D6) δ174.8 (cyclic =C-S), 155.7 (cyclic N=C-N-), 134.1, 112.2 (C=C), 24.5–23.6 (4 CH_2); and MS (*m/z*): M^{+1} 200 (5%), 199 (100%). Analysis for $C_{10}H_{10}N_2O_2S$ (222.05) revealed calcd.: % C, 54.04; H, 4.54; N, 12.60; S, 14.42, and found: % C, 54.15; H, 4.43; N, 12.35; S, 14.61.

2,4-Dichloro-5,6,7,8-tetrahydrobenzo[4,5]thieno[2,3-d] pyrimidine (8)

Overall, 1 mmol of compound 7 was refluxed with phosphorus oxychloride for 6 h until a clear solution appeared at end of reaction (TLC test), and then it was evaporated and poured into ice water, and an organic layer was extracted by DCM, dried over sodium sulfate, and then evaporated to get compound 8.

Product 8 was separated as colorless crystals, with yield 65% (EtOH); M.P. of 177–179°C; IR (KBr, cm^{-1}): 1620 (C=C), 1600 (C=N), 743 (C-Cl); 1H NMR (500 MHz, DMSO-D6) δ2.84–2.68 (m, 4H, 2 CH_2), 1.72–1.65 (m, 4H, 2 CH_2); ^{13}C NMR (125 MHz, DMSO-D6) δ174.5 (cyclic =C-S), 155.2 (cyclic N=C-N-), 134.2, 112.3 (C=C), 24.4–23.5 (4 CH2); and MS (*m/z*): M+: 258, 241 : 243 : 243 (100, 30, 10%). Analysis for $C_{10}H_8C_{l2}N_2S$ (259.15) revealed calcd.: % C, 46.35; H, 3.11; Cl, 27.36; N, 10.81; S, 12.37, and found: % C, 46.54; H, 3.02; Cl, 27.59; N, 10.49; S, 12.25.

2-Amino-N-phenyl-4,5,6,7-tetrahydrobenzo[b]thiophene-3-carboxamide (9)

Overall, 1 mmol of compound 1 was fused with 1 mmol of aniline at 100°C for 5 h. The reaction mixture was cooled and dissolved in methanol, and the formed residue was filtered, dried, and crystallized from ethanol to afford compound 9.

Product 9 was separated as pale yellow crystals, with yield 80% (EtOH); M.P. of 163–165°C; IR (KBr, cm^{-1}): 3300, 3230, 3150 (NH, NH2), 1679 (C=O), 1612 (C=C); ^{1}H NMR (500 MHz, DMSO-D6) δ8.01 (s, 2H, NH2), 7.79–7.12 (m, 5H, CHarom.), 7.02 (s, 1H, NH), 2.86–2.67 (m, 4H, CH2), 1.73–1.61 (m, 4H, 2 CH_2); ^{13}C NMR (125 MHz, DMSO-D6) δ161.8 (C=O), 152.7 (cyclic =C S-), 136.5, 134.1,

129.9, 122.2, 120.9, 105.6 (CHarom.), 25.5–23.6 ($4CH_2$); and MS (*m/z*): M^{+1} 272 (20%), 273 (100%). Analysis for $C_{15}H_{16}N_2O_S$ (272.10) revealed calcd.: % C, 66.15; H, 5.92; N, 10.29; S, 11.77, and found: % C, 66.20; H, 5.80; N, 10.35; S, 11.45.

2-Methyl-3-phenyl-5,6,7,8-tetrahydrobenzo[4,5]thieno[2,3-d]pyrimidin-4(3H)-one (10)

In 30 ml acetic anhydride, compound 9 (1 mmol) was dissolved and stirred at reflux temperature for 15 h. The formed solid product was allowed to cool, filtered of and crystallized from ethanol to afford 10.

Product 10 was separated as yellow crystals, with yield 78% (EtOH); M.P. 207-209°C; IR (KBr, cm^{-1}): 1669 (C=O), 1612 (C=C), 1601 (C=N); ^1H NMR (500 MHz, DMSO-D6) δ7.49–7.12 (m, 5H, CHarom.), 2.85–2.68 (m, 4H, CH_2), 2.54 (s, 3H, CH_3), 1.74–1.65 (m, 4H, 2 CH_2); ^{13}C NMR (125 MHz, DMSO-D6) δ160.8 (C=O), 154.8 (C-Me), 150.7 (cyclic =C-S-), 137.5, 133.1, 129.2, 128.2, 111.1 (CHarom.), 25.5–23.6 ($4CH_2$), 21.5 (CH_3); and MS (*m/z*): M^{+1} 296 (5%). Analysis for $C_{17}H_{16}N_2O_S$ (296.10) revealed calcd.: % C, 68.89; H, 5.44; N, 9.45; S, 10.82, and found: % C, 68.72; H, 5.35; N, 9.29; S, 10.70.

2-Phenyl-5,6,7,8-tetrahydrobenzo[4,5]thieno[2,3-d] [1,2,3] triazin-4(3H)-one (11)

Overall, 1 mmol of sodium nitrite was dissolved in water (7 ml) at 0°C and added drop-wise to stirred solution of 1 mmol of compound 9, which was dissolved in acetic acid (40 ml) in ice bath. The stirring was continued to 2 h (TLC). The formed residue was filtered, dried, and crystallized from acetic acid to afford 11.

Product 11 was separated as brown crystals, with yield 55% (EtOH); MP 243–245°C; IR (KBr, cm^{-1}): 1660 (C=O), 1650 (N=N), 1612 (C=C); 1H NMR (500 MHz, DMSO-D6) δ7.35–7.15 (m, 5H, CHarom.), 2.85–2.68 (m, 4H, CH_2), 1.74–1.65 (m, 4H, 2 CH_2); 13C NMR (125 MHz, DMSO-D6) δ159.8 (C=O), 152.7 (cyclic =C-S-), 138.5, 137.1, 129.9, 128.7, 126.3, 120.1 (CHarom.), 27.5–25.6 ($4CH_2$); and MS (*m/z*): M+1284 (40%). Analysis for $C_{15}H_{13}N_3OS$ (283.08) revealed calcd.: % C, 63.58; H, 4.62; N, 14.83; S, 11.31, and found: % C, 63.81; H, 4.45; N, 14.70; S, 11.51.

2-Mercapto-3-phenyl-5,6,7,8-tetrahydrobenzo [4,5]thieno [2,3-d]pyrimidin-4(3H)-one (12)

Overall, 1 mmol of compound 9 was added to 1 mmol of carbon disulfide and dissolved in NaOEt solution (50 ml) with stirring at reflux temperature for 12 h. The reaction was cooled and poured into cold water, and diluted hydrochloric acid was added to neutralize at pH=8.9. The formed residue was filtered, dried, and crystallized from ethanol to yield 12.

Product 12 was separated as brown crystals, with yield 70% (EtOH); M.P. 340–342°C; IR (KBr, cm^{-1}): 2569 (SH), 1659 (C=O), 1612 (C=C), 1585 (C=N); ^1H NMR (500 MHz, DMSO-D6) δ7.37–7.16 (m, 5H, CHarom.), 2.85 (s, 1H, SH), 2.80–2.68 (m, 4H, CH_2), 1.74–1.65 (m, 4H, 2 CH_2); ^{13}C NMR (125 MHz, DMSO-D6) δ154.8 (C=O), 150.7 (cyclic =C-S-), 137.4, 133.2, 129.3, 128.5, 120.1 (CHarom.), 25.6–23.4 (4CH2); and MS (*m/z*): M^{+1} 314 (20%). Analysis for $C_{16}H_{14}N_2OS_2$ (314.05) revealed calcd.: % C, 61.12; H, 4.49; N, 8.91; S, 20.39, and found: % C, 61.25; H, 4.55; N, 8.79; S, 20.45.

(2R,3R, 5R,6S)-2-(acetoxymethyl)-6-((4-oxo-3-phenyl-3,4,5,6,7,8-hexahydrobenzo[4,5]thieno[2,3-d]pyrimidin-2-yl)thio)tetrahydro-2H-pyran-3,4,5-triyl triacetate (13)

A mixture of 12 (1 mol) in aqueous potassium hydroxide solution (5 mol, 2 ml) in absolute acetone (20 ml) was added to 2,3,4,6-O-acetyl-α-D-glucopyranosyl bromide (4.10 g, 0.01 mol) and stirred at room temperature for 10 h. The solvent was evaporated under reduced pressure. The formed solid product was washed with water to remove potassium bromide and crystallized from ethanol to afford 13.

Product **13** was separated as yellow crystals, with yield 60% (EtOH); M.P. of 191–193°C; IR (KBr, cm^{-1}): 1752 (C=O), 1612 (C=C), 1600 (C=N), 1210–1035 (C–O–C); ^1H NMR (500 MHz, DMSO-D6) δ7.43–7.15 (m, 5H, CHarom.), 5.55 (dd, *J*=9.5, 2.7 Hz, 1H, cyclic CH), 5.43 (d, *J*=0.9 Hz, 1H, cyclic CH-S), 5.22 (dd, *J*=2.6, 1.1 Hz, 1H, cyclic CH), 4.88 (dd, *J*=9.6, 6.1 Hz, 1H, cyclic CH), 4.45–4.40 (m, 1H, Ha, CH2), 4.30 (d, *J*=6.1 Hz, 1H, cyclic CH), 4.10–4.02 (m, 1H, Hb, CH2), 2.86–2.75 (m, 2H, CH2), 2.62–2.55 (m, 2H, CH2), 2.02, 1.99, 1.97, 1.95 (4s, 12H, 4 OAc), 1.73–1.61 (m, 4H, 2 CH_2); ^{13}C NMR (125 MHz, DMSO-D6) δ172.8 (3 C=O), 165.4 (C=O), 155.4 (C=O), 150.7 (cyclic =C-S-), 134.1, 130.1, 129.1, 128.6, 119.9, 112.2 (CHarom.), 74.2, 73.5, 70.5, 70.2, 69.6 (5 pyran C), 60.5 (CH_2), 25.2–23.5 (2 CH_2), 21.3–20.6 (CH_3); and MS (*m/z*): M+644 (20%). Analysis for $C_{30}H_{32}N_2O_{10}S_2$ (644.15) revealed calcd.: % C, 55.89; H, 5.00; N, 4.35; S, 9.95, and found: % C, 55.75; H, 5.12; N, 4.53; S, 9.74.

3-Phenyl-2-(((2S,3R,5S,6R)-3,4,5-trihydroxy-6-(hydroxymethyl) tetrahydro-2H-pyran-2-yl)thio)-5,6,7,8-tetrahydrobenzo[4,5]thieno[2,3-d]pyrimidin-4(3H)-one (14)

The forgoing procedure of compound **6** was applied to compound **14**.

Product **14** was separated as yellow crystals, with yield 50% (EtOH); M.P. of 175–177°C; IR (KBr, cm^{-1}): 3401–3335 (very broad OH), 1680 (C=O), 1610 (C=C), 1588 (C=N); ^{1}H NMR (500 MHz, DMSO-D6) δ7.40–7.10 (m, 5H, CHarom.), 5.40 (d, *J*=5.5 Hz, 1H, OH), 5.31 (d, *J*=5.6 Hz, 1H, OH), 5.10 (d, *J*=5.1 Hz, 1H, OH), 4.55 (d, *J*=6.1 Hz, 1H, OH), 4.47–4.35 (m, 1H, Ha, CH_2), 4.11–4.04 (m, 1H, Hb, CH_2), 3.67–3.88 (m, 5H, CH pyran), 2.85–2.76 (m, 2H, CH_2), 2.61–2.56 (m, 2H, CH_2),1.73–1.61 (m, 4H, 2 CH_2); ^{13}C NMR (125 MHz, DMSO-D6) δ171.8 (3 C=O), 169.4 (C=O), 156.4 (C=O), 152.7 (cyclic =C-S-), 134.1, 133.5, 132.5, 128.6, 120.6, 119.9, 112.2 (CHarom.), 74.3, 73.8, 70.2, 70.1, 69.9 (5 pyran C), 60.2 (CH_2), 25.5–23.6 (2 CH_2), 21.3–20.5 (CH_3); and MS (*m/z*): M^{+1} 476 (5%). Analysis for $C_{22}H_{24}N_2O_6S_2$ (476.11) revealed calcd.: % C, 55.45; H, 5.08; N, 5.88; S, 13.45, and found: % C, 55.59; H, 5.15; N, 5.72; S, 13.33.

Cytotoxic evaluation

Cell culture

Three cancer cell lines MCF-7 (human breast cancer cell line), HepG-2 (human liver cancer cell line), PC-3 (human prostate cancer cell lines), and human normal melanocyte cell line (HFB4) were obtained from the National Cancer Institute (Cairo University), Cairo, Egypt. The cells were preserved at 37°C in DMEM (Dulbecco's modified Eagle's medium), 10% heat-inactivated fetal calf serum (GIBCO), streptomycin (100 µg/ml), and penicillin (100 U/ml) in humidified CO_2 atmosphere (5%).

Cell viability/fast screening

Cells were seeded in 96-well plates. The newly synthesized compounds were applied on the three cell lines to test their cytotoxic activity. The compounds were tested in two different concentrations (0.01 and 10 µM). The two working solutions were prepared using the complete medium. Three technical replicates were carried out for each concentration. The treated cells were incubated at 37°C for 48 h. Afterward, the cell viability was identified by MTT assay. The comparison was performed between the treated cells to the positive control (reference drug) and the negative control (DMSO). The assays were performed in biological replicates.

IC_{50} determination

The compounds with significant activity were chosen for further analysis. Each compound in different concentrations (5, 10, 15, 25, 50, and 100 µg/ml) was tested. The working solutions were prepared using the complete medium. Three technical replicates were performed for each concentration. The treated cells were incubated at 37°C in 5% CO_2 for 48 h. The viability of the cells was identified using MTT assay. IC_{50} values (50% inhibitory concentration) were calculated with a four-parameter logistic function and presented in mean. The assay was performed in biological replicates.

MTT assay

The cells were washed with PBS (50 µl) and then the PBS was discarded. Afterward, 50 µl of MTT working solution was applied to each well, and the cells were incubated at 37°C for 15â 30 min. The cells were examined microscopically for formazan (dark blue precipitate) development. This formazan production is directly proportional to the viable cell number and inversely proportional to the degree of cytotoxicity [19–22]. The supernatant was discarded from each well, and the formazan was dissolved using DMSO. The developed color absorbance was determined by an automated plate reader at 570 nm with a background wavelength of 670 nm. The results were presented in percentage to the values obtained from untreated cells (negative control).

System preparation

The crystal structures of the human thymidylate synthase complexed with raltitrexed, solved at resolution of 1.9Å, was retrieved from the protein data bank with codes 1HVY [23]. These structures were then prepared for molecular dynamics (MD) studies using UCSF Chimera [24]. Using PROPKA, pH was fixed and optimized to 7.5 [25]. Compounds 5, 10, and 14 were drawn using ChemBioDraw Ultra 12.1 [26]. Altogether, all three prepared systems were subjected to 50 ns.

MD simulations as described in the simulation section.

Molecular dynamic simulations

The integration of MD simulations in biological systems' study enables exploring the physical motion of atoms and molecules that cannot be easily accessed by any other means [27]. The insight extracted from performing this simulation provides an intricate perspective into the biological systems' dynamical evolution, such as conformational changes and

molecule association [27]. The MD simulations of all systems were performed using the GPU version of the PMEMD engine present in the AMBER 18 package [28].

The partial atomic charge of each compound was calculated with ANTECHAMBER's General Amber Force Field (GAFF) technique [29]. The Leap module of the AMBER 18 package implicitly solvated each system within an orthorhombic box of TIP3P water molecules within 10Å of any box edge. The Leap module was used to neutralize each system by incorporating Na+ and Cl- counter ions. A 2000-step initial minimization of each system was carried out in the presence of a 500 kcal/mol applied restraint potential, followed by a 1000-step full minimization using the conjugate gradient algorithm without restraints.

During the MD simulation, each system was gradually heated from 0 to 300 K over 500 ps, ensuring that all systems had the same amount of atoms and volume. The system's solutes were subjected to a 10 kcal/mol potential harmonic constraint and a 1 ps collision frequency. Following that, each system was heated and equilibrated for 500 ps at a constant temperature of 300 K. To simulate an isobaric-isothermal (NPT) ensemble, the numbers of atoms and pressure within each system for each production simulation were kept constant, with the system's pressure maintained at 1 bar using the Berendsen*et al.* [30] barostat.

For 50 ns, each system was MD simulated. The SHAKE method was used to constrain the hydrogen bond atoms in each simulation. Each simulation used a 2 fs step size and integrated an SPFP precision model. An isobaric-isothermal ensemble (NPT) with randomized seeding, constant pressure of 1 bar, a pressure-coupling constant of 2 ps, a temperature of 300 K, and a Langevin thermostat with a collision frequency of 1 ps was used in the simulations.

Post-molecular dynamics analysis

After saving the trajectories obtained by MD simulations every 1 ps, the trajectories were analyzed using the AMBER18 suite's CPPTRAJ [31] module. The Origin [32] data analysis program and Chimera [24] were used to create all graphs and visualizations.

Thermodynamic calculation

The Poisson-Boltzmann or generalized Born and surface area continuum solvation (MM/PBSA and MM/GBSA) approach has been found to be useful in the investigation of a wide range of nucleic acid systems [33–36]. The receptor–ligand complex molecular simulations used by MM/GBSA and MM/PBSA compute rigorous statistical-mechanical binding free energy within a defined force field [37,38].

Binding free energy averaged over 500 snapshots was extracted from the entire 50 ns trajectory. The estimation of the change in binding free energy (ΔG) for each molecular species (complex, ligand, and receptor) can be represented as follows [39]:

$$\Delta G_{bind} = G_{complex} - G_{ligand} \quad (1)$$

$$\Delta G_{bind} = E_{gas} + G_{sol} - T.S \quad (2)$$

$$E_{gas} = E_{int} + E_{vdw} + E_{ele} \quad (3)$$

$$G_{sol} - G_{G.B.} + G_{S.A.} \quad (4)$$

$$GS.A. = \gamma SASA \quad (5)$$

The terms E_{gas}, E_{int}, E_{ele}, and E_{vdw} symbolize the gas-phase energy, internal energy, coulomb energy, and van der Waals energy, respectively. The Egas was directly assessed from the FF14SB force field terms. Solvation-free energy (Gsol) was evaluated from the energy involvement from the polar states (GGB) and nonpolar states (G). The nonpolar solvation free energy (GSA) was determined from the Solvent Accessible Surface Area [40] using a water probe radius of 1.4Å. In contrast, solving the G.B. equation assessed the polar solvation (GGB) contribution. Items S and T symbolize the total entropy of the solute and temperature, respectively.

Drug-like parameter computation and ADMET profiling

For computing drug-like features from 2D chemical structures of the aforementioned compounds, the Molinspiration (http://www.molinspiration.com/) online tool set and OSIRIS property explorer were employed [41–44].

Human intestinal absorption (HIA%), Caco-2 cell permeability (nm/s), MDCK (Medin-Darbey Canine Kidney Epithelial Cells) cell permeability (nm/s), plasma protein binding (percent), blood–brain barrier penetration (C. brain/C. blood), and Pgp inhibition were among the pharmacokinetic parameters calculated using the pre-ADMET online server (https://pre-admet.bmdrc.kr/) [45].

The Molinspiration online (http://www.molinspiration.com/) tool kit [46] was used to estimate the bioactivity of synthesized compounds, and OSIRIS property explorer was used to calculate toxicity parameters such as mutagenicity, tumorigenicity, irritating effects, and reproductive effects [47].

Results and discussion

Chemistry

Thieno[2,3-*d*] pyrimidinone moiety has been functionalized with thiol group to conjugate with sugar units to enhance the biological activities of the target compounds. Two synthetic pathways have been followed to introduce the thiol group into thieno[2,3-*d*] pyrimidinone.

Compound (**3**) has been prepared by reacting ethyl 2-amino-4,5,6,7-tetrahydrobenzo[*b*]thiophene-3-carboxylate (**1**) with benzoyl isothiocyanate, which acts as a good leaving group that accelerates the ring closure in the presence of sodium ethoxide (Scheme1). Mercaptothieno[2,3-d] pyrimidinone (**3**) reacted with 2,3,4,6-*O*-acetyl-α-*D*-glucopyranosyl bromide (**4**) afforded the corresponding 2-mercaptothieno [2,3-*d*] pyrimidinone glucose conjugate (**5**). Compound (**5**) deacetylated *via* stirring at room temperature in methanol in the presence of triethylamine yielded the corresponding the free thieno[2,3-*d*]pyrimidinone glucose conjugate (**6**) (Scheme 1). Structures of compounds (**1-6**) were elucidated by using spectroscopic and analytical testes (*cf.* Experimental). Thus, in 1H NMR spectrum of compound **6** as an example, OH protons were detected as doublet at 5.41–4.56 and at *δ*3.67–3.88 as multiplet (5H, CH pyran), which was also confirmed using 13C NMR, which exhibited signals at *δ*171.8 (3 C=O), 169.4 (C=O), 156.4 (C=O), 152.7 (cyclic =C-S-), 134.1, 119.9, 112.2 (3 quaternary C), 74.3, 73.8, 70.2, 70.1, and 69.9 (5 pyran C).

For further reaction and for developing new derivatives with different linkers, compound **1** was reacted with urea to afford 5,6,7,8-tetrahydrobenzo [4,5] thieno [2,3-*d*] pyrimidine-2,4-diol (**7**). Two chloro groups have been introduced into the peripheries of the thieno[2,3-*d*] pyrimidine moiety (**8**) *via* reaction of compound **7** with phosphorous pentachloride (Scheme 2).

Compound **12** has been also prepared to utilize the thiol reactive center through the reaction of compound **1** with aniline to afford 2-amino-*N*-phenyl-4,5,6,7-tetrahydrobenzo[*b*]thiophene-3-carboxamide (**9**), which was followed by reaction with carbon disulfide in the presence of sodium ethoxide to get **12** (Scheme 2). A direct approach to obtain thieno[2,3-*d*] pyrimidine (**10**) was by reacting compound **9** with acetic anhydride. Moreover, diazotization of compound **9** in the presence of sodium nitrite and acetic acid yielded 3-phenyl-5,6,7,8-tetrahydrobenzo [4,5] thieno[2,3-*d*][1,2,3] triazin-4(3*H*)- one (**11**) (Scheme 2). Structures of compounds **7–12** were proved using spectroscopic analysis (IR, NMR, and M.S.) (*cf.* Experimental).

2-Mercapto-3-phenylthieno[2,3-d] pyrimidinone (**12**) was reacted with 2,3,4,6-*O*-acetyl-α-D-glucopyranosyl

Scheme 1

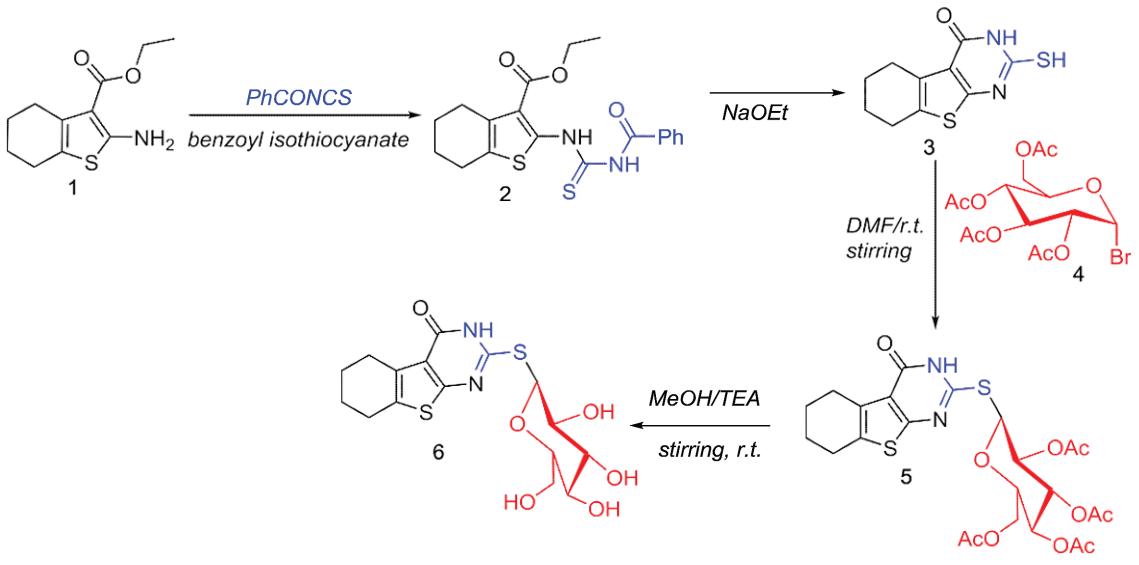

Synthesis of compounds 2, 3, 5, and 6.

Scheme 2

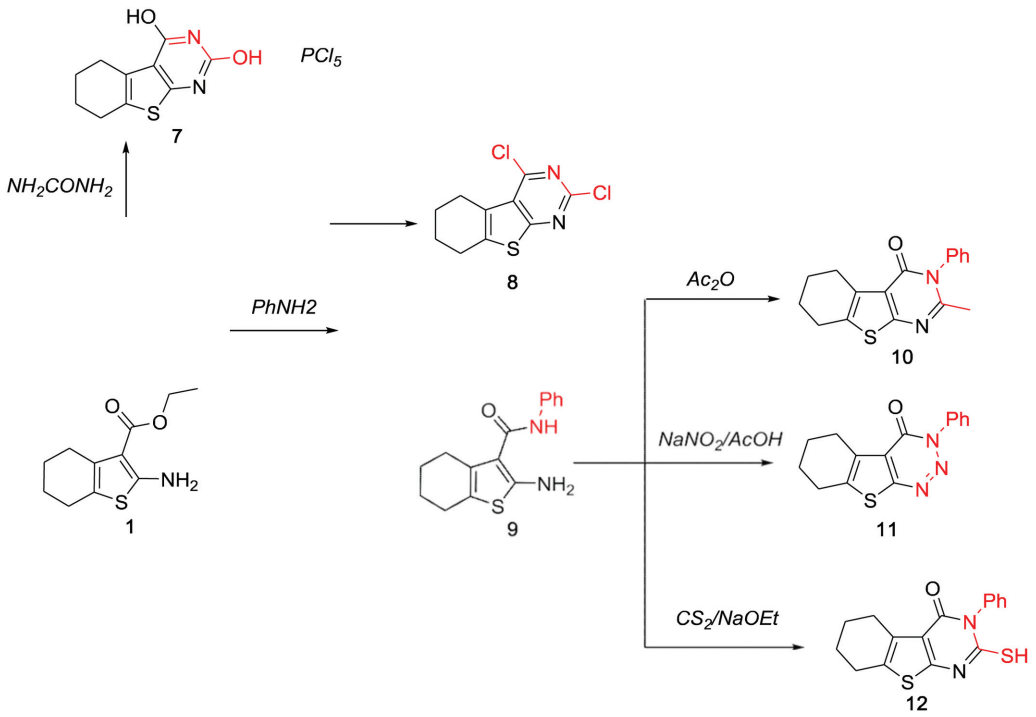

Synthesis of compounds 7–12.

Scheme 3

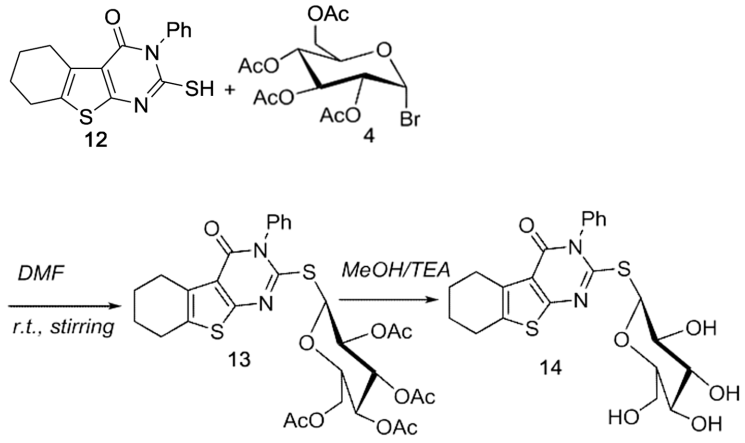

Synthesis of compounds 13 and 14.

bromide to afford the corresponding 2-mercapto-3-phenyl thieno[2,3-*d*] pyrimidinone glucose conjugates (**13**). Furthermore, compound **12** deacetylated in the presence of triethylamine in methanol yielded the corresponding free thieno[2,3-*d*] pyrimidinone glucose conjugate (**14**) (Scheme 3).

Cytotoxic activities

Fast screening

Quick screening was done to see how the newly synthesized compounds affected the viability of cancer cell lines MCF-7, HepG-2, and PC-3, as well as a normal cell line (human normal melanocyte, HFB4), in comparison with a recognized anticancer drug: MTT test for 5-fluorouracil. Most of the compounds revealed a remarkable decrease in the cell viability of at least one of the three cell lines. The effect of the new compounds on the MCF-7 and HepG-2 cancer cell lines is shown in Fig. 1. Our results indicated that most of the tested compounds exhibited no activity against the growth of HFB4, the normal human skin melanocytes cell line. Furthermore, all compounds were analyzed to find out their IC_{50} values.

Figure 1

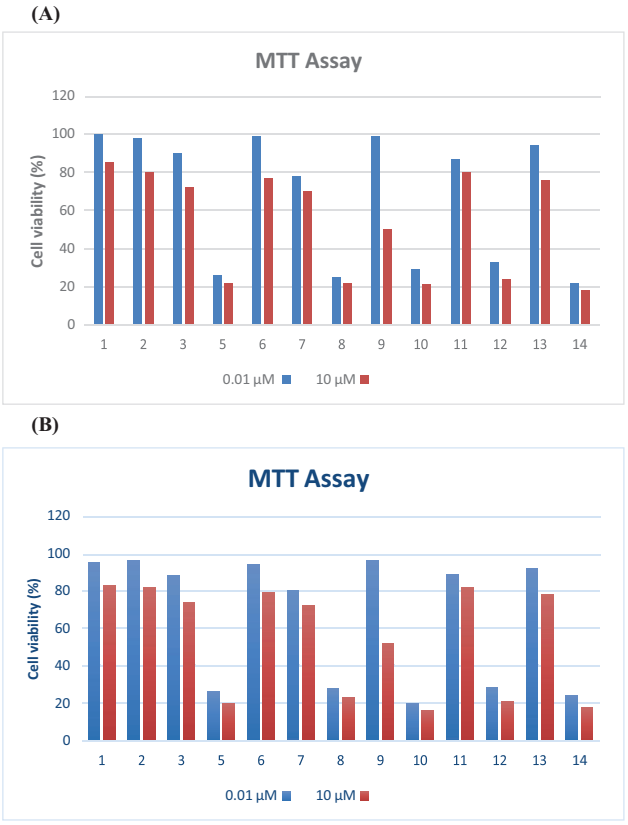

MCF-7 (A) and HepG-2 (B) cell viability after 48 h treatment with the synthesized derivatives.

Table 1 IC_{50} value (µM) by MTT assay of the three cell lines, 48 h of treatment

Compd. No.	Cell line		
	MCF-7	HEPG-2	PC-3
Solvent	34.65±5.43	32.86±0.11	36.6±5.24
1	37.5±0.35	33.02±0.40	32.86±0.11
2	14.87±1.15	12.16±2.23	16.44±1.74
3	15.61±1.86	17.6±0.02	22.24±5.87
5	4.65±0.83	5.77±0.99	22.2±1.08
6	23.05±1.17	32.86±0.11	40.43±1.1
7	19.02±0.20	15.61±1.86	33.12±2.01
8	6.21±2.10	7.23±0.98	29.8±1.73
9	35.59±3.10	45.19±1.31	36.3±10.68
10	5.43±1.05	4.42±1.32	36.37±6.87
11	23.05±1.17	43.11±11.28	23.61±2.79
12	7.00±0.88	7.9±0.90	31.74±1.34
13	25.15±6.26	26.84±0.43	28.38±1.64
14	3.25±1.07	5.1±11.28	27.41±2.68
5-Flurouracil	3.97±0.10	4.27±0.58	5.05±0.66

IC_{50} determination

The IC_{50} determination was used to determine the cytotoxicity of all drugs because they were all active in the fast-screening experiment. The obtained viabilities were used to plot the dose-dependent response of the cell lines and establish the $^{IC}_{50}$ for each chemical.

Table 1 reveals that in both MCF-7 and HepG-2 cancer cell lines, the majority of the chemicals significantly reduced cell viability. Because almost all of the chemicals inhibited cell growth, they were all further investigated to discover their IC_{50}. The MTT assay for the studied substances revealed that the

majority of them had IC_{50} values ranging from 3.25 to 43.11 g/ml (Table 1). The chemicals' cytotoxic potential varies by cell type (Fig. 2). The cytotoxicity of the newly synthesized compounds was assessed in the normal human skin melanocytes cell line HFB4 to see if they are exclusively active in cancer cells or if they have toxicity toward normal cells as well. The findings demonstrated that the majority of the chemicals examined had no effect on the proliferation of HFB4, a normal human skin melanocyte cell line. Many of the chemicals examined have impressive cytotoxic activity against the MCF-7 breast cancer cell line and the HepG-2 liver cancer cell line. Compounds (5, 8, 10, 12, and 14) showed antiproliferative action with IC_{50} values that were similar to the reference medicine (IC_{50} 4.6, 6.2, 5.4, 7, and 3.25 g/ml, respectively, compared with 3.97 g/ml for 5-fluorouracil).

Only modest to moderate activity was seen in the remaining compounds. In a similar manner, cytotoxic activity of the tested compounds against human liver HepG-2 cancer cell lines revealed that compounds 5, 8, 10, 12, and 14 were similar to the standard drug (IC_{50} values 5.770±99, 7.230±98, 4.421±32, 7.90±90, and 5.111±28 g/ml, respectively, vs. 4.270.58 g/ml for 5-fluorouracil). The rest of the

Figure 2

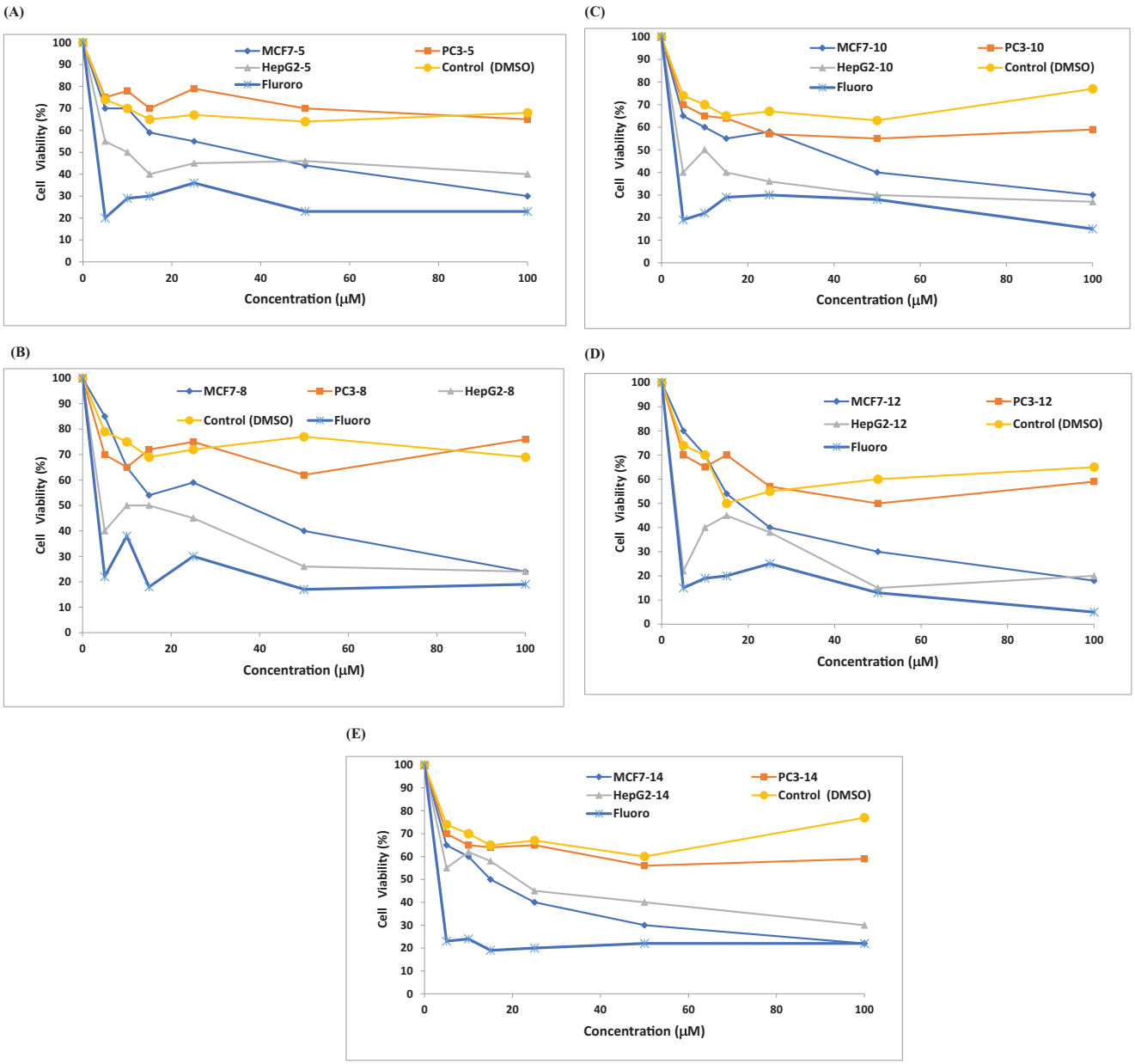

Dose-dependent response of MCF-7, HepG-2, and PC-3 cancer cell lines treated with compound 4 (a), compound 8 (b), compound 10 (c), compound 12 (d), and compound 14 (e) determined by MTT assay (48 h).

substances examined showed rather minor action. The newly synthesized compounds (5, 8, 10, 12, and 14) displayed cytotoxicity and growth inhibitory action on both breast and liver cancer cell lines, as previously indicated. On a prostate cancer cell line, there was some cytotoxicity and growth inhibition efficacy (PC-3). Table 1 shows that (a) the cytotoxic activity of the studied compounds against breast cancer (MCF-7) declines in the following order: 14>5>10 >8>12

(b) the evaluated drugs' cytotoxic activity against liver cancer (HepG-2) declines in the following order: 10>14>5>8>12.

Molecular dynamic and system stability

To study putative ligands' inhibitory effectiveness and interactions with the human thymidylate synthase targets, MD simulations were carried out. To trace disturbed motions and avoid artifacts that may occur during the simulation, system stability must be validated. Root-mean-square deviation was used to analyze the systems' stability during the 50 ns simulations in this study.

The recorded average root-mean-square deviation values for all frames of systems 5-TS, 10-TS, and 14-TS were 1.47Å, 1.62Å, and 1.39 Å, respectively (Fig. 3a). These results revealed that the 14-T.S. complex system acquired a relatively more stable conformation than the other studied system.

Assessing protein structural flexibility upon ligand binding is crucial for analyzing residue behavior and their relationship with the ligand during MD simulation [48].

The effect of inhibitor binding toward the individual targets was examined using the root-mean-square fluctuation algorithm on the human thymidylate synthase residues throughout 50 ns simulations.

The computed average root-mean-square fluctuation values were 0.99Å, 1.10Å, and 0.89Å for 5-TS, 10-TS, and 14-TS, respectively. Overall residue fluctuations of individual systems are represented in Fig. 3b. These values revealed that 14 has a lower residue fluctuation than the other systems inhibition.

Binding interaction mechanism based on binding free energy calculation

The structural basis for a ligand's activity is its binding to a specific pharmacological target. As a result, using free binding energy calculations to predict the thymidylate synthase receptor–ligand-binding affinities is a promising method for finding novel protein inhibitors [49]. The binding free energies were calculated using the MM-GBSA tool in AMBER18 by extracting snapshots from the systems' trajectories. Table 2 shows that all of the computed energy components (with the exception of Gsolv) had large negative values, indicating positive interactions.

Binding free energy (ΔG_{bind}) values −30.63, −23.18 and −44.97 kcal/mol were obtained to interact with thymidylate synthase residues with compounds **5**, **10,** and **14**, respectively. This indicates a more favorable binding of compound 14 toward thymidylate synthase

Figure 3

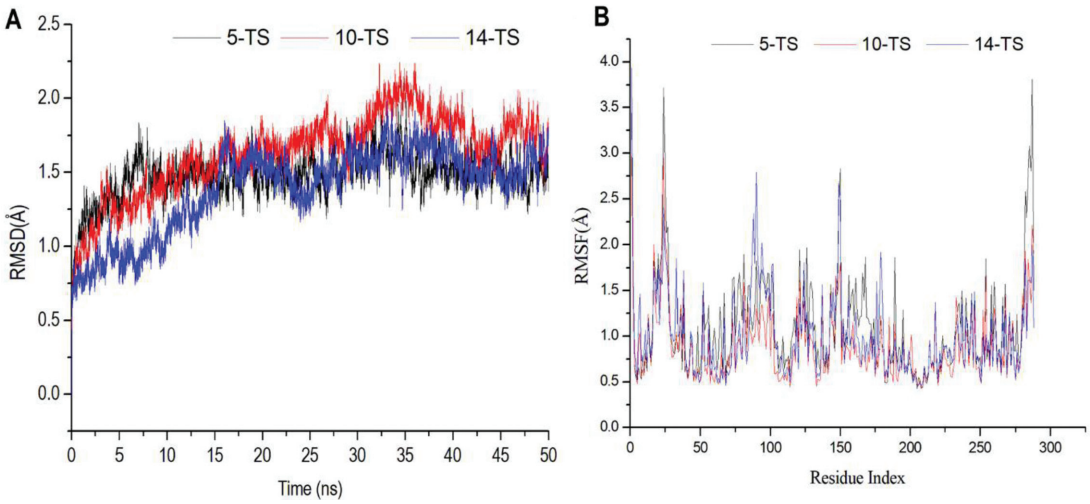

(a) RMSD of ligand interactions 5-TS, 10-TS, and 14-TS. (b) RMSF of each residue of the protein backbone Ca atoms. RMSD, root-mean-square deviation; RMSF, root-mean-square fluctuation.

Table 2 The calculated energy binding for (5, 11, and 14) against the human thymidylate synthase receptor

	Energy components (kcal/mol)				
Complex	$^{\Delta E}$vdW	$^{\Delta E}$elec	$^{\Delta G}$gas	$^{\Delta G}$solv	$^{\Delta G}$bind
5	−48.48±0.19	−19.50±0.27	−67.98±0.37	37.34±0.24	−30.63±0.18
10	−32.69±0.12	-7.59 ±0.12	−40.28± 0.20	17.09±0.10	−23.18±0.13
14	−59.61±0.14	−39.26 ±0.39	−98.88±0.49	53.09±0.27	−44.97±0.24

ΔEele, electrostatic energy; ΔEvdW, van der Waals energy; $^{\Delta G}$bind, calculated total binding free energy; ΔGsolv, solvation free energy.

receptor than compounds 5 and 10. It is interesting to see how the calculated binding free energy correlated to the experimentally determined MIC values in a good manner.

A close inspection of the individual energy contribution reveals that the more positive Vander Waals energy components drive interactions of compounds 5, 10, and 14 with the human thymidylate synthase residues, resulting in the reported binding free energies. Substantial binding free energy values were observed in the gas phase for all of the inhibition processes with values up to −67.98, −40.28, and −98.88 kcal/mol, respectively (Table 2).

Identification of the critical residues responsible for ligand binding

The total energy involved when 5, 10, and 14 derivatives bind these enzymes was further decomposed into the involvement of each site residues to get deeper insights into critical residues involved in the inhibition of thymidylate synthase receptor. From Fig. 4, the major favorable contribution of 5 derivative to thymidylate synthase receptor is predominantly observed from residues Asp 23 (−37.93 kcal/mol), Thr 25 (−12.65 kcal/mol), Glu 61 (−42.12 kcal/mol), Leu62 (−12.13 kcal/mol), Leu 63 (−14.84 kcal/mol), Leu 172 (−8.67 kcal/mol), Leu195 (−8.66 kcal/mol), Gly196 (−6.04 kcal/mol), Asn200 (−67.08 kcal/mol), Thr225 (−7.11 kcal/mol), Leu 226 (−12.02 kcal/mol), Gly 227 (−5.69 kcal/mol), and Asp228 (−45.44 kcal/mol).

On the contrary, the major favorable contributions of thymidylate synthase inhibition by 10 derivative were predominantly observed from residues Arg24 (−159.86 kcal/mol), Thr25 (−11.36 kcal/mol), Glu 61 (−40.95 kcal/mol), Leu 62 (−12.53 kcal/mol), Leu 63 (−15.21 kcal/mol), Asp 84 (−46.63 kcal/mol), Asn 86 (−66.11 kcal/mol), Gly87 (−4.39 kcal/mol), Val 108 (−5.06 kcal/mol), Gly 110 (−3.20 kcal/mol), Ser 190 (−7.14 kcal/mol), Gly 191 (−5.24 kcal/mol), Asp 192 (−44.07 kcal/mol), Gly 194 (−5.84 kcal/mol), Leu 195 (−11.62 kcal/mol), Asn 200(−68.20 kcal/mol), and Val 287 (−79.32 kcal/mol).

Finally, the major favorable contribution of 14 derivative to thymidylate synthatase receptor is predominantly observed from residues Lys 21 (−15.89 kcal/mol), Asp 22 (−50.43 kcal/mol), Asp 23 (−39.86kcal/mol), Thr25 (−17.01 kcal/mol), Asp 48 (−46.98 kcal/mol), Asn 86 (−64.09 kcal/mol), Leu 92 (−17.17 kcal/mol), Gln 188 (−40.75 kcal/mol), Ser 190 (−6.33 kcal/mol), Gly 191 (−5.96 kcal/mol), Asp 192 (−44.53 kcal/mol), Asn 200 (−65.44 kcal/mol), Leu 233 (−9.60 kcal/mol), and Asn 234 (−79.86 kcal/mol).

Analysis of the molecular mechanism and ligand binding mode

Figure 5 shows that the Tyr 232 residue of the thymidylate synthase catalytic active binding site has formed hydrogen bonds with the oxygen atoms of the pyrimidine ring in compound 5, with the sulfur atom of the thiophene ring in compound 10, and with the sulfur atom of the thiolpyrimidine ring of compound 14.

Furthermore, Histidine 230, a pharmacophoric hotspot, has created a hydrogen bond contact with both compounds 5 and 14. It is worth noting that eight other hydrophobic ligands interact with Arg 24, Thr 25, Ile 82, Leu 166, His 176, Gln 188, Asp 192, and Met 282 in the hydrophobic accessible pocket, stabilizing the energetically favorable ligands.

A total of 23 residues were found at the binding of the thymidylate synthase-5 complex, whereas 22 residues were seen in the thymidylate synthase-10 complex. Finally, a total number of 24 residues were shown in the thymidylate synthase-14 complex.

In silico prediction of ADMET properties

Lipinski's rule of five, topological polar surface area, aqueous solubility, and the number of rotatable bonds are all estimated in Table 3. The absorption rates in the human intestine ranged from 82.16 to 99.67%, showing that the compounds generated had a moderate to good absorption capability and supported their interaction with target cells (Table 4). In vitro Caco-2 cell permeability in the range of 1.96–55.70 nm/s and in vitro MDCK cell

Figure 4

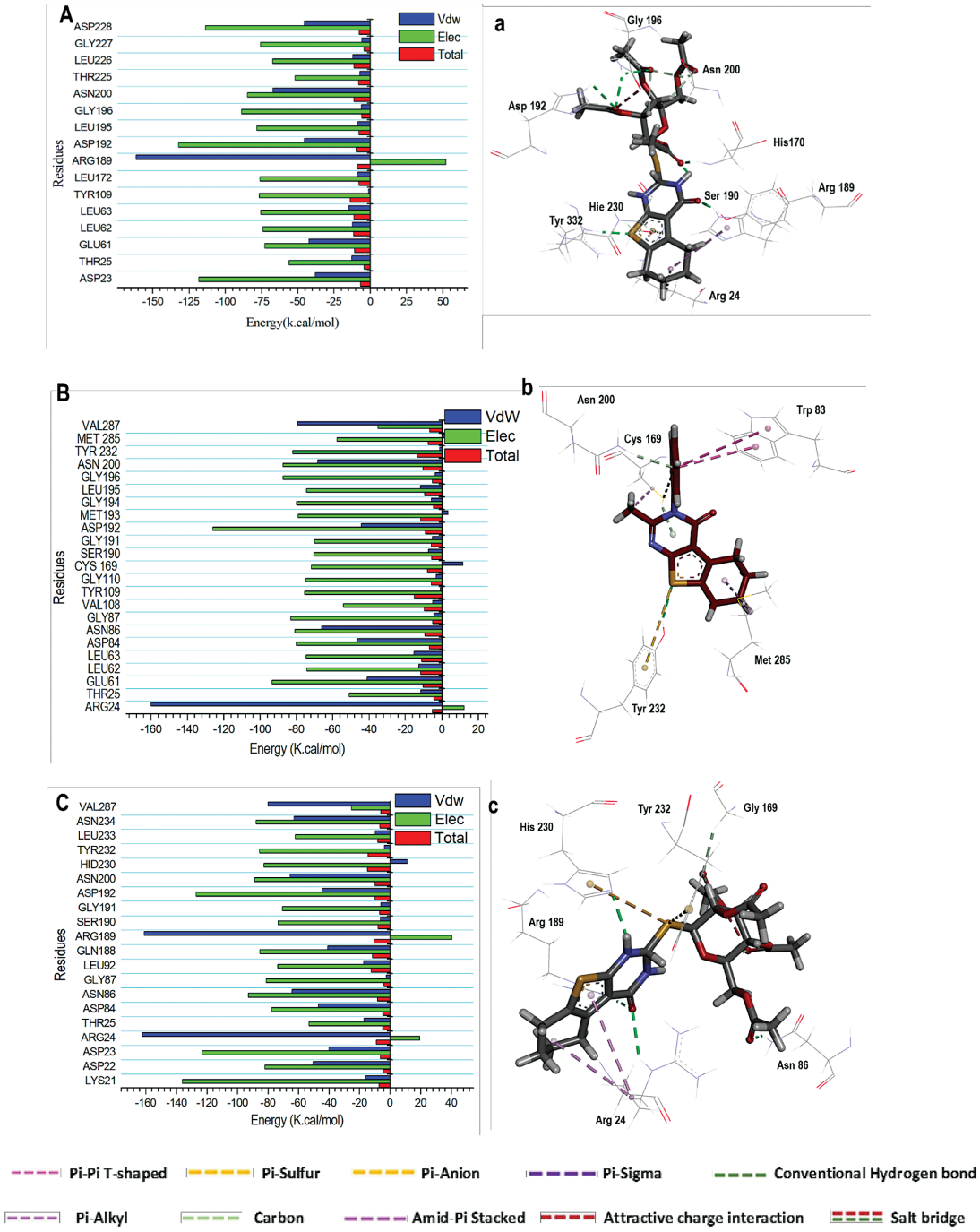

Molecular visualization of interaction between 5 with thymidylate synthase (a), between 10 and thymidylate synthase (b) and between 14 and thymidylate synthase (c).

permeability in the range of 1.51–60.94 nm/s were used to determine the low permeability of target compounds with the concerned cell line. The generated compounds have a modest ability to bind to proteins, ranging from 54.91 to 100%. In vivo blood–brain barrier penetration ranges from 0.08 to 2.79, indicating low to moderate distribution with medium to good penetration capacity (Table 4). Table 5 lists the bioactivity and toxicity risk ratings of synthesized drugs.

Conclusion

In this study, some of the new compounds were successfully synthesized, and their structures were estimated using IR, ^{1}H NMR, and ^{13}C NMR. 2-mercapto thieno[2,3-d] pyrimidinone [15] was successfully conjugated with different reagents to get novel derivatives. These compounds were tested for biological activity against three different human cancer

Figure 5

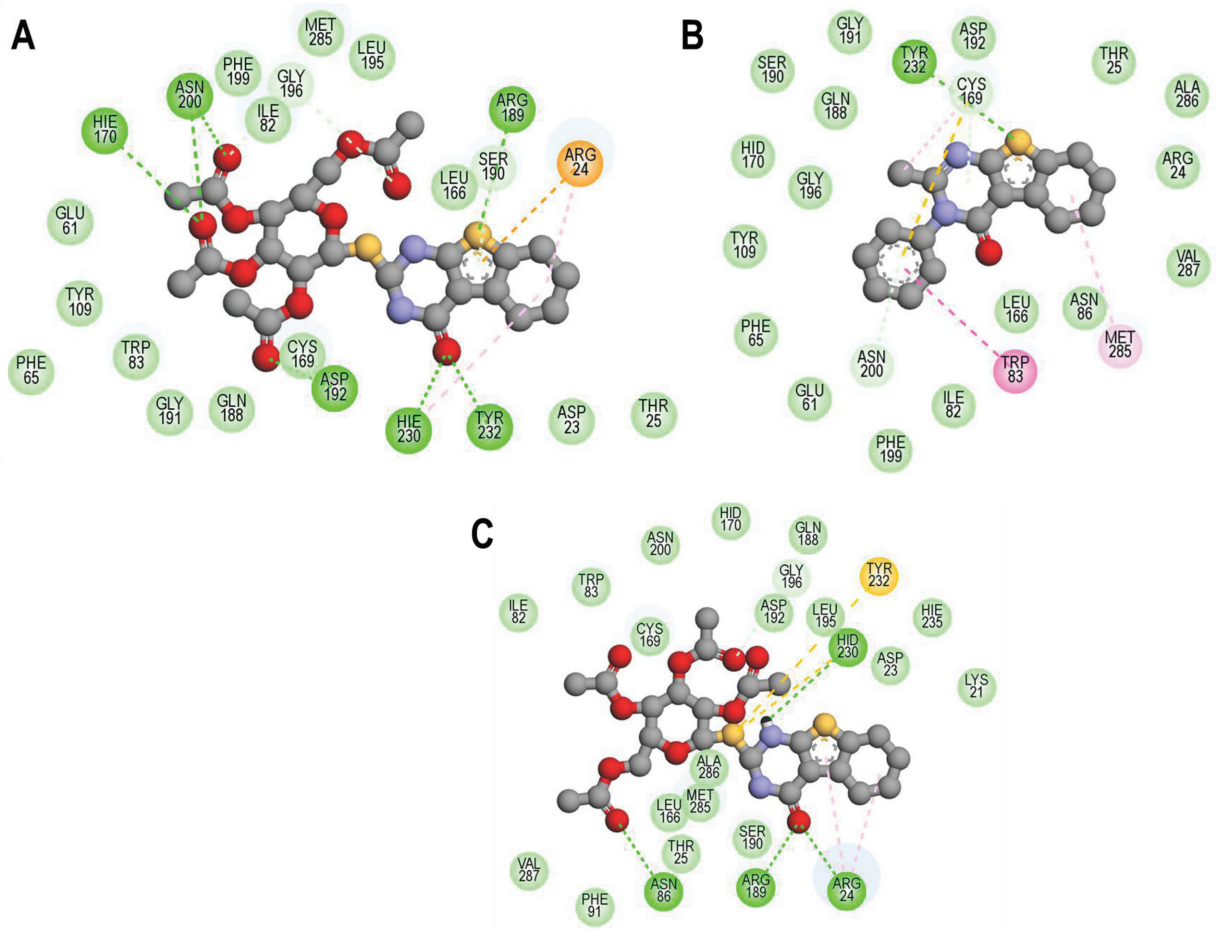

The two-dimensional binding confirmation between the thymidylate synthase at the catalytic active binding site residues with compound 5 (a), compound 10 (b), and compound 14 (c).

Table 3 Topological polar surface area, aqueous solubility, number of rotatable bonds, and calculated Lipinski's rule of five for the synthesized compounds

Comp.	miLog $_P$a	Log S[b] (mol/l)	TPSA[c] (Å^2)	MW[d]	nON[e]	nOHNH[f]	nvoilation[g]	nroth	Vol
1	2.52	−3.38	52.33	225.31	3	2	0	3	203.74
2	4.11	−5.37	67.43	388.51	5	2	0	7	335.51
3	2.63	−4.39	45.75	238.34	3	1	0	0	192.59
5	3.45	−5.06	160.21	568.63	12	1	2	11	470.25
6	1.07	−3.42	135.90	400.48	5	5	0	3	324.21
7	2.48	−3.99	66.24	222.27	4	2	0	0	182.84
8	4.27	−4.79	25.78	259.16	2	0	0	0	193.78
9	3.20	−4.46	55.12	272.37	3	3	0	2	245.20
10	3.35	−4.77	34.90	296.39	3	0	0	1	263.28
11	3.12	−4.62	47.79	283.36	4	0	0	1	242.56
12	3.98	−5.86	34.90	314.44	3	0	0	1	264.38
13	4.24	−5.54	149.35	644.72	12	0	2	12	542.04
14	1.86	−4.90	125.04	476.58	8	4	0	4	396.00

[a]Logarithm of partition coefficient between n-octanol and water (miLogP). [b]Solubility (Log S). [c]Topological polar surface area (TPSA). [d]Molecular weight (MW). [e]Number of hydrogen bond acceptor (nON). [f]Number of hydrogen bond donor (nOHNH). [g]Number of violations (nvoilations). [h]Number of rotatable bonds (nrot).

cell lines: MCF-7, HepG-2, and PC-3, as well as a normal cell line (human normal melanocyte, HFB4), in contrast to the well-known anticancer drug, and they showed promising cytotoxic activities against the human breast cancer cell lines (MCF-7) and human hepatocellular carcinoma cell line (HepG-2) at very

Table 4 ADME property values of synthesized compounds using pre-ADMET online server

Comp.	Human intestinal absorption (HIA, %)	*Invitro*Caco-2 cell permeability (nm/s)	*In vitro* MDCK cell permeability (nm/s)	*In vitro* plasma protein binding (%)	*In vivo* blood–brain barrier penetration (C. brain/C. blood)	Pgp_ inhibition
1	94.732272	15.9532	50.3257	100.00	1.1586	None
2	95.916714	36.2924	1.51964	90.82	0.156687	Inhibitor
3	94.570252	29.0618	45.1253	100.00	0.823232	None
5	95.187752	28.4157	0.0722784	74.59	0.159301	None
6	56.364250	1.17676	0.180025	54.910	0.0468972	None
7	91.586657	1.96701	43.6854	100.00	0.776777	Inhibitor
8	97.409133	56.3807	60.9491	100.00	2.79539	Inhibitor
9	94.586051	7.60847	31.534	100.00	0.115178	None
10	97.704505	39.6093	20.6656	100.00	0.0405888	Inhibitor
11	98.939857	24.0302	44.313	98.93	0.0187373	Inhibitor
12	99.670981	55.7008	13.0958	100.00	0.104474	Inhibitor
13	97.970952	34.8107	16.1162	87.248	0.16216	Inhibitor
14	82.167654	1.96487	0.0661658	100.00	0.0850908	None

Table 5 Bioactivity and toxicity risk of synthesized compounds

Comp.	GPCR ligand	Ion-channel modulator	Kinase inhibitor	Nuclear receptor ligand	Protease inhibitor	Mutagenic	Tumorigenic	Reproductive effective	Irritant
1	−1.04	−1.27	−1.50	−1.69	−1.63	None	None	None	None
2	−0.82	−1.05	−0.77	−1.06	−0.93	None	None	High	None
3	−1.30	−1.03	−1.43	−2.72	−1.81	None	None	None	None
5	−0.32	−0.66	−0.63	−0.94	−0.54	None	None	None	None
6	−0.33	−0.70	−0.69	−1.25	−0.65	None	None	None	None
7	−0.68	−0.43	−0.85	−1.96	−1.20	None	High	None	None
8	−0.49	−0.47	−0.86	−1.49	−1.19	None	None	None	None
9	−0.50	−1.00	−0.54	−1.14	−0.93	High	None	None	None
10	−0.28	−0.49	−0.84	−1.43	−0.73	High	None	None	None
11	−0.60	−0.76	−0.81	−1.38	−0.99	High	Moderate	None	None
12	−0.75	−0.80	−0.86	−1.66	−1.11	High	None	None	None
13	−0.49	−1.12	−0.88	−1.20	−0.59	High	None	None	None
14	−0.37	−0.64	−0.61	−1.12	−0.65	High	None	None	None

low concentrations. MD simulation followed by MM-GBSA calculation was correlated to the cytotoxic effect, and compound 14 illustrated the highest MM-GBSA value (-20.38) and the best cytotoxic effect.

Acknowledgements

The authors are grateful to National Research Center and Beni-Suef University, Egypt, for supporting the work.

Financial support and sponsorship

Nil.

Conflicts of interest

There are no conflicts of interest.

References

1 Asif M. Diverse chemical and pharmacological properties of triazine compounds. Int J Heterocy Chem 2019; 9:49–79.

2 Zhuang J, Ma S. Recent development of pyrimidine-containing antimicrobial agents. Chem Med Chem 2020; 15:1875–1886.

3 Aly AA, Behalo MS. Efficient synthesis of thieno [2, 3-d] pyrimidines and related fused systems. J Chem Res 2010; 34:571–575.

4 He Z-X., Zhao T-Q., Gong Y-P., Zhang X, Ma L-Y., Liu H-M. Pyrimidine: a promising scaffold for optimization to develop the inhibitors of ABC transporters. Eur J Med Chem 2020; 200:112458.

5 Lagoja IM. Pyrimidine as constituent of natural biologically active compounds. Chem Biodivers 2005; 2:1–50.

6 Rashad A, Ali M. Synthesis and antiviral screening of some thieno [2, 3-d] pyrimidine nucleosides. Nucleos Nucleot Nucl Acids 2006; 25:17–28.

7 Elrazaz EZ, Serya RA, Ismail NS, Abou El Ella DA, Abouzid KA. Thieno [2, 3-d] pyrimidine based derivatives as kinase inhibitors and anticancer agents. Future J Pharm Sci 2015; 1:33–41.

8 Ameen MA, Ahmed EK, Mahmoud HI, Ramadan M. Synthesis and screening of phosphodiesterase 5 inhibitory activity of fused and isolated triazoles based on thieno [2, 3-d] pyrimidines. J Heterocycl Chem 2019; 56:1831–1838.

9 Viswanatha GL, Priyadarshini BJ, Krishnadas N, Janardhanan S, Rangappa S, Hanumanthappa S. Synthesis and antihistaminic activity of 3H-benzo [4, 5] thieno [2, 3-d][1, 2, 3] triazin–4–ones. Saudi Pharm J 2012; 20:45–52.

10 Elrayess R, Abdel Aziz YM, Elgawish MS, Elewa M, Elshihawy HA, Said MM. Pharmacophore modeling, 3D-QSAR, synthesis, and anti-lung cancer evaluation of novel thieno [2, 3-d][1, 2, 3] triazines targeting EGFR. Arch Pharm 2020; 353:1900108.

11 Cascioferro S, Parrino B, Spano V, Carbone A, Montalbano A, Barraja P, Diana P, Cirrincione G. Synthesis and antitumor activities of 1, 2, 3–triazines and their benzo-and heterofused derivatives. Eur J Med Chem 2017; 142:74–86.

12 Ashour HM, Shaaban OG, Rizk OH, El-Ashmawy IM. Synthesis and biological evaluation of thieno [2′, 3′: 4, 5] pyrimido [1, 2-b][1, 2, 4] triazines and thieno [2, 3–d][1, 2, 4] triazolo [1, 5–a] pyrimidines as anti-inflammatory and analgesic agents. Eur J Med Chem 2013; 62:341–351.

13 Aly AA, Ramadan M, Mohamed AM, Ishak EA. Thieno [2, 3-d] pyrimidines in the synthesis of new fused heterocyclic compounds of prospective antitumor and antioxidant agents (Part II). J Heterocycl Chem 2012; 49:1009–1018.

14 Saravanan J, Mohan S, Roy JJ. Synthesis of some 3-substituted amino-4, 5-tetramethylene thieno [2, 3-d][1, 2, 3]–triazin–4 (3H)-ones as potential antimicrobial agents. Eur J Med Chem 2010; 45:4365–4369.

15 Aly AA, Ishak EA, Ramadan M, Germoush MO, El-Emary TI, Al-Muaikel NS. Recent report on thieno [2, 3-d] pyrimidines. Their preparation including microwave and their utilities in fused heterocycles synthesis. J Heterocycl Chem 2013; 50:451472.

16 Gewald K, Schinke E, Bottcher H. Heterocycles from acidic nitriles, VIII 1) 2-amino-thiophenes from active methylene-nitriles, carbonyl and sulfur compounds. Carbonylverbindungen und Schwefel Chem Ber 1966; 99:94–100.

17 Sharkawy K, Sehrawi H, Ibrahim RA. The reaction of 2-amino-4, 5, 6, 7–tetrahydrobenzo [b] thiophenes with benzoyl-isothiocyanate: synthesis of annulated thiophene derivatives and their antitumor evaluations. Inter J Org Chem 2012; 2:126–134.

18 Gomha SM. A facile one-pot synthesis of 6, 7, 8, 9–tetrahydrobenzo [4, 5] thieno [2, 3-d]-1, 2, 4–triazolo [4, 5-a] pyrimidin-5-ones. Monat Chem 2009; 140:213–220.

19 Covell DG, Huang RW. Anticancer medicines in development: assessment of bioactivity profiles within the National Cancer Institute anticancer screening data. Mol Cancer Ther 2007; 6:2261–2270.

20 Takimoto CH. Anticancer drug development at the U.S. National Cancer Institute. Cancer Chemother Pharmacol 2003; 52:29–33.

21 Rubinstein L, Shoemaker R, Paull K, Simon R, Tosini S, Skehan P, *et al.* Comparison of in vitro anticancer-drug-screening data generated with a tetrazolium assay versus a protein assay against a diverse panel of human tumor cell lines. J Nat Cancer Inst 1990; 82:1113–1117.

22 Madhuri S, Pandey G. Some anticancer medicinal plants of foreign origin. Curr Sci 2009; 96:779–783.

23 Phan J, Koli S, Minor W, Dunlap RB, Berger SH, Lebioda LJB. Human thymidylate synthase is in the closed conformation when complexed with dUMP and raltitrexed, an antifolate drug. Biochemistry 2001; 40:1897–1902.

24 Pettersen EF, Goddard TD, Huang CC, Couch GS, Greenblatt DM, Meng EC, Ferrin TE. UCSF Chimera—a visualization system for exploratory research and analysis. J Comput Chem 2004; 25:1605–1612.

25 Li H, Robertson AD, Jensen JHJPS. Function, bioinformatics, very fast empirical prediction and rationalization of protein pKa values. Prot Strcut Funct Bioinformat 2005; 61:704–721.

26 Halford B. Reflections on chemdraw. Chem Eng News Arch 2014; 92:26–27.

27 Hospital A, Goñi JR, Orozco M, Gelpí JL. Molecular dynamics simulations: advances and applications. J Adv App Bioinformat Chem 2005; 8:37.

28 Lee T-S., Cerutti DS, Mermelstein D, Lin C, LeGrand S, Giese TJ, *et al.* GPU-accelerated molecular dynamics and free energy methods in Amber18: performance enhancements and new features. J Chem Info 2018; 58:2043–2050.

29 Wang J, Wang W, Kollman PA, Case DA. Automatic atom type and bond type perception in molecular mechanical calculations. J Molgraph Model 2006; 25:247–260.

30 Berendsen HJ, Postma JV, van Gunsteren WF, DiNola A, Haak J. Molecular dynamics with coupling to an external bath. J Chem Phys 1984; 81:3684–3690.

31 Roe DR, Cheatham IIITE. Software for processing and analysis of molecular dynamics trajectory data. J Chem Theory Comput 2013; 9:3084–3095.

32 Seifert E. OriginPro 9.1: scientific data analysis and graphing softwaresoftware review. Austin, Texas, United States: ACS Publications; 2014.

33 Srinivasan J, Cheatham TE, Cieplak P, Kollman PA, Case DA. Continuum solvent studies of the stability of DNA,RNA, and phosphoramidate – DNA helices. J Am Chem Soc 1998; 120:9401–9409.

34 Kollman PA, Massova I, Reyes C, Kuhn B, Huo S, Chong L, *et al.* Calculating structures and free energies of complex molecules: combining molecular mechanics and continuum models. Acc Chem Res 2000; 3:889–897.

35 Srinivasan J, Miller J, Kollman PA, Case DA. Continuum solvent studies of the stability of RNA hairpin loops and helices. J Biomol Strct 1998; 16:671–682.

36 Cheatham IIITE, Srinivasan J, Case DA, Kollman PA. Molecular dynamics and continuum solvent studies of the stability of polyG-polyC and polyA-polyT DNA duplexes in solution. J Biomol Strct 1998; 16:265–280.

37 Drissi M, Benhalima N, Megrouss Y, Rachida R, Chouaih A, Hamzaoui F. Theoretical and experimental electrostatic potential around the m-nitrophenol molecule. Molecules 2015; 20:4042–4054.

38 Wang L. Molecular Dynamics - Studies of Synthetic and Biological Macromolecules [Internet]. London: IntechOpen; 2012; 446. [cited 2022 Aug 07], Available from: https://www.intechopen.com/books/2265 doi: 10.5772/2652

39 Hou T, Wang J, Li Y, Wang W. Assessing the performance of the MM/PBSA and MM/GBSA methods. 1. The accuracy of binding free energy calculations based on molecular dynamics simulations. J Chem Inf Model 2010; 51:69–82.

40 Sitkoff D, Sharp KA, Honig B. Accurate calculation of hydration free energies using macroscopic solvent models. J Phys Chem 1994; 98:1978–1988.

41 El-Gohary NS, Shaaban MI. Antimicrobial and antiquorum-sensing studies. Part 3: synthesis and biological evaluation of new series of [1, 3, 4] thiadiazoles and fused [1, 3, 4] thiadiazoles. Arch Pharm 2015; 348:283–297.

42 Lipinski CA, Lombardo F, Dominy BW, Feeney PJ. Experimental and computational approaches to estimate solubility and permeability in drug discovery and development settings. Adv Drug Delv Rev 1997; 23:3–25.

43 Cardoso MF, Rodrigues PC, Oliveira MEI, Gama IL, da Silva IM, Santos IO, *et al.* Synthesis and evaluation of the cytotoxic activity of 1, 2–furanonaphthoquinones tethered to 1, 2, 3–1H-triazoles in myeloid and lymphoid leukemia cell lines. Eur J Med Chem 2014; 84:708–717.

44 Veber DF, Johnson SR, Cheng H-Y., Smith BR, Ward KW, Kopple KD. Molecular properties that influence the oral bioavailability of drug candidates. J Med Chem 2002; 45:2615–2623.

45 Murugavel S, Kannan D, Bakthadoss M. Experimental and computational approaches of a novel methyl (2E)-2-{[N-(2-formylphenyl)(4-methylbenzene) sulfonamido] methyl}-3-(4-chlorophenyl) prop-2-enoate: a potential antimicrobial agent and an inhibition of penicillin-binding protein. J Mol Struct 2016; 1115:33–54.

46 Balam SK, Krishnammagari SK, Soora Harinath J, Sthanikam SP, Chereddy SS, Pasupuleti VR, *et al.* Synthesis of N-(3-picolyl)-based 1, 3, 2λ5–benzoxazaphosphinamides as potential 11β-HSD1 enzyme inhibitor Med Chem Res 2015; 24:1119–1135.

47 de Oliveira KN, Souza MM, Sathler PC, Magalhães UO, Rodrigues CR, Castro HC, *et al.* Sulphonamide and sulphonyl-hydrazone cyclic imide derivatives: antinociceptive activity, molecular modeling and in silico ADMET screening. Arch Pharm Res 2012; 35:17131722.

48 Machaba KE, Mhlongo NN, Soliman ME. Cell biochem. biophys. induced mutation proves a potential Target for T.B. Therapy 2018; 76:345–356.

49 Cournia Z, Allen B, Sherman W. Relative binding free energy calculations in drug discovery: recent advances and practical considerations. J Chem Inf Model 2017; 57:2911–2937.